DOI 10.24425/aee.2024.150889

Maximum power point tracking controller for photovoltaic system based on chaos quantum particle swarm optimization – moth-flame optimization hybrid model

ZILI WANG ✉, WEILU YUAN

College of Electromechanical Engineering
Anyang Vocational and Technical College
Anyang 455000, China
e-mail: {✉ ZiliWang2021/Yuanwl2023}@163.com

(Received: 09.01.2024, revised: 22.08.2024)

Abstract: To convert photovoltaic arrays to solar energy in a more efficient way, this paper has proposed a maximum power point tracking controller model based on the chaotic quantum particle swarm-mothballing hybrid algorithm. First, the optimization of the particle swarm algorithm is designed to solve defects, such as premature maturity by using the quantum and chaotic strategies. The mothballing algorithm is introduced to help the model find global optimization-seeking more quickly. After that, further optimization was made to operate the tracking model in both offline and real-time parameters. The conductivity increment method and the perturbation observation method were adopted to effectively track the model under different temperatures and light intensities. Finally, the simulation and analysis experiments were carried out on the Simulink platform. The study's proposed maximum power point tracking controller achieved a steady-state accuracy $\eta 2$ of 99.84%. In summary, the study has proposed a hybrid intelligent algorithm with extraction of internal parameters. The maximum power point tracker based on the proposed method is proved to be both effective and accurate.

Key words: maximum power point tracking, moth-flame optimization, particle swarm optimization, photovoltaic systems

1. Introduction

With the depletion of non-renewable resources, research has gradually shifted to find renewable energy sources to meet our ever-increasing need for power. As a highly reliable and clean energy source. solar energy has received much attention from the public. The energy in solar radiation is

equivalent of 250 million barrels of oil per day, making solar energy one of the most important energy source for human beings [1]. When the sun shines onto a solar panel, energy from the sunlight is absorbed by the PV cells in the panel. This energy creates electrical charges that move in response to an internal electrical field in the cell, causing electricity to flow. Generally, multiple cell arrays are required to generate a large power output. The output is nonlinear and can be affected by temperature or light intensity. When a PV array cell is exposed to a uniform light, there is just one peak in the electricity it has generated, which serves as the point of maximum power. To maximize power generation efficiency, a tracking controller is used to ensure that the cell operates near that point [2]. Photovoltaic arrays are often installed on rooftops, facades, and some open areas. When a solar panel is shaded by trees or other objects, the current that cannot flow around weak cells will eventually concentrate in some cells, causing them to overheat and potentially melt. As a result, the hotspot effect occurs. This can be solved by adding diodes. However, this will lead to a multi-peak curve of the battery output, making it hard for the tracking controller to track the maximum power. Most contemporary tracking algorithms can accurately track the maximum power point, but they often demand a large volume of data, which slow down the operation of the model. Therefore, we need to design a fast and accurate maximum power tracking algorithm. [3] For example, incremental conductance (INC) and perturb and observe (P&O) are commonly used in MPPT technology. The INC method extracts the maximum power point by the incremental conductance of the solar panel. In other words, the maximum power point can be found when the value is negative. Compared with the P&O method, the INC method has a higher accuracy and can determine the maximum power point under rapidly changing atmospheric conditions, but it requires more complex calculation and control. The P&O method finds the maximum power point based on the voltage and current disturbance of the solar panel. Compared with the INC method, the P&O system faces high oscillation especially under unstable environmental conditions and its response speed is slow. Therefore, it is necessary to optimize MPPT technology to combine both methods' advantages and overcome the disadvantages, so as to achieve optimal system performance and tracking effect. Owners of photovoltaic installations, can gain significant benefits from MPPT algorithm's optimization. Photovoltaic systems can maximize power generation, boost energy conversion efficiency, lower energy loss, and convert more solar energy into electricity by continuously tracking the maximum power point. After the optimization, the photovoltaic system can have a longer lifespan, and the owners of the photovoltaic system can recover their capital much faster and earn more economic benefits. Therefore, the tracking model proposed by the study is based on both the quantum particle swarm and mothballing algorithms. The study has four parts. The first section introduced the development of photovoltaic array batteries. The second section combined and optimized the particle swarm algorithm and the mothballing algorithm to design a tracker. The third section conducted experiments to simulate and analyze maximum power tracking controllers. The fourth section is a summary of the experimental data.

2. Related works

Photovoltaic (PV) technology is a branch of electrical energy conversion technologies in solar energy. To maximize its efficiency to generate power, we need to track the maximum power point. Asoh D.A. *et al*. believe that it was very important to track the maximum power point of the

PV panels, because it could improve the efficiency and reduce the cost. Therefore, they used IC algorithms and the model with irradiation and temperature variations during the modeling of the tracker. Then, a simulation test was carried out to verify the effectiveness in the rapidly changing environment. According to the results, their algorithm can constantly track the MPP of the PV system and quickly respond to the changes in temperature and irradiance within 2 seconds [4]. Rerhrhaye *et al*. believed that the volatility of solar energy and climatic factors may hinder the integration of PV into the power grid. Therefore, they proposed a control technique based on the maximum power point (MPP) tracking. They added a complex function to the PV system using an ant colony optimization algorithm. Several performance metrics were also adopted to determine the optimal control parameters and evaluate the system performance. According to the simulation results, the method is both stable and robust [5]. Mishra *et al*. proposed a self-tuning incremental conductance MPP tracking algorithm that changes the perturbation frequency and the step size in the photovoltaic system. They applied this algorithm on an Arduino Mega-2560 microcontroller and compared it with the traditional fixed conductance MMP tracking algorithm. According to the results, the optimized algorithm had a steady state and a better dynamic performance. Its oscillations were fewer and its tracking response was faster [6]. Dehghani *et al*. proposed a fuzzy logic controller to determine the optimal duty cycle and the maximum power point of the photovoltaic power generation system. It was based on particle swarm optimization and genetic algorithms, which analyzed power and voltage variations. The method has been proved to have a better performance in the MATLAB/Simulink software [7].

To keep the output voltage of PV panels at the maximum power point, Lei *et al*. improved the variable step-size perturbation and observation algorithm based on partition. In this way, the PV energy harvesting would be more stable. The power generation system's operating area is divided into different parts. The small step size is used near the MPP to speed up the tracking, while the bigger and fixed step size is used away from the MPP. According to the simulation results, the algorithm has fewer oscillations and its tracking speed is two times faster [8]. To enable the self-powered wireless sensor networks, Zhang *et al*. proposed a PV power source, of which the structure was simple and the tracking efficiency was high. The new technique combined both traditional MPP tracking algorithm and the fixed-step-size MPP tracking method, which was done by sampling and pulse-width modulation. To determine the variable step size of the perturbation, it also compared the difference between the observed and theoretical currents. According to the experimental results, the tracking efficiency could be as high as 90% to 92% [9]. Gharpure *et al*. improved the perturbation observation MPP tracking technique for thermoelectric generators. The proposed technique reduced oscillations and improved the steady state and dynamic efficiency. Compared with the conventional perturbation observation algorithm, the algorithm's efficiency was 2%–2.5% higher. [10]. Yan *et al*. proposed an adaptive estimator based on the Kalman filter to track the MPPT of the hydrogen fuel cell in the hybrid UAV. To make it work better, a mathematical model and real-time parameter adjustment tools were added. Compared with traditional P&O and other particle swarm optimization methods, its tracking error was reduced by 2.83% and 1.10%, respectively [11]. To improve the performance of the PV power generation systems that were connected to the grid, L. Wang *et al*. proposed a new three-port energy router with an optimized control strategy. They developed six working modes to manage energy in a more efficient way by using DC links, such as the staggered boost structure [12].

Although tracking effect can be optimized by most MPP trackers, high speed always comes at the cost of accuracy. For example, P&O method takes simple steps to optimize the system, but the oscillation, which was an undesirable phenomenon, was difficult to overcome, and its accuracy is not enough. The INC method, like the P&O method, is also affected by oscillations under rapidly changing conditions, thus requiring a higher measurement accuracy. The derivative peak approach needs precise numerical differentiation of the power-voltage curve, which can be affected by the noise and result in position errors. The AI method requires a large sample size to learn, with a very high calculation cost. To have a better tracking effect, the methods above need to be integrated. Many studies have been conducted to optimize the step size control and improve the model's accuracy. However, the proposed methods have not lowered the calculation costs. Based on the chaotic quantum-behaved particle swarm algorithm and the mothballing algorithm, this paper has designed an internal parameter extraction algorithm to optimize MPP tracking of the model.

3. Real-time MPPT tracking model design based on CQPSO-MFO hybrid algorithm

To make solar PV power generation more efficient, we constructed a maximum power tracker. An internal-parameter-based tracking model was proposed. The internal parameters of the PV array were extracted by the particle swarm algorithm and mothballing algorithm model with the quantum chaos strategy. To extract the internal parameters offline and in real-time, we introduced the Lambert W function and combined it with the conductivity increment method and the perturbation observation method. Finally, the tracking of the maximum power point of the PV array was conducted.

3.1. Maximum power tracking hybrid model construction based on CQPSO-MFO

Photovoltaic (PV), which uses its photovoltaic reaction to convert energy into electricity, is a common technology for solar power generation. To obtain the desired output power, a module or array that consists of multiple cells are used. To improve the PV array's stability, the optimal operating point needs to be found using maximum power point tracking (MPPT). Most MPPT controllers cannot track internal parameters of the PV cell, such as the photogenerated current, the ideal diode factor, and the resistance of the series or parallel connections [13]. The non-linear characteristics of the PV cells require the actual data to be fitted to get the internal parameters. The study identifies parameters through the explicit function method, in which we use the Lambert W function to solve the explicit output equations and narrow the gap between the real and theoretical values. First, we introduced a particle swarm optimization (PSO) algorithm, the particles of which are shown in (1) [14].

$$\begin{cases} x_{id}^{k+1} = x_{id}^{k} + v_{id}^{k+1}, \quad (1 \le i \le N, 1 \le d \le D) \\ v_{id}^{k+1} = \omega v_{id}^{k} + c_1 r_1 (x_{p\text{best}\_id} - x_{id}^{k}) + c_2 r_2 (x_{g\text{best}\_d} - x_{id}^{k}) \end{cases}. \tag{1}$$

In (1), x_{id}^{k}/x_{id}^{k} denotes the position and velocity of the particle i in the k-th iteration in d dimension; ω represents the inertia weight; c_1/c_2 is the acceleration factor; r_1/r_2 is an arbitrary number in the interval (0, 1); $x_{p\text{best}\_id}$ shows the optimal position of the particle; $x_{g\text{best}\_d}$ denotes the optimal position of the particle swarm; N is the number of particles; and D is the number of particle dimensions. Figure 1 shows the detailed process.

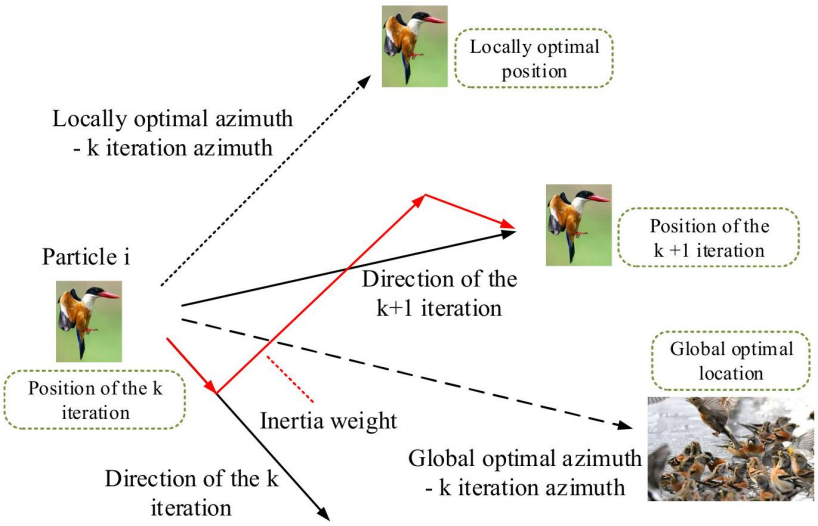

Fig. 1. Iteration update form of particle swarm

As the traditional PSO algorithm tends to fall into local optimum, we have introduced quantum particle swarm optimization (QPSO) to transform the original orientation vectors. In this optimization, the wave function is used, as shown in Eq. (2) [15].

$$x_{id}^{k} = \begin{cases} x_{p\text{best}\_id} - \beta \left| x_{m\text{best}\_d} - x_{id}^{k} \right| \ln\left(\frac{1}{u}\right), & u \geqslant 0.5 \\ x_{p\text{best}\_id} + \beta \left| x_{m\text{best}\_d} - x_{id}^{k} \right| \ln\left(\frac{1}{u}\right), & u < 0.5 \end{cases}. \tag{2}$$

In (2), u/φ represents an arbitrary number in the interval (0, 1); $x_{m\text{best}\_d}$ is the average optimal position of the particle swarm in the dimension d; and β is the expansion coefficient. However, the optimized algorithm has a significantly lower proficiency to control the parameters. To ensure that the model can completely search the region, we have introduced chaos quantum particle swarm optimization (CQPSO), as shown in Eq. (3).

$$\begin{cases} x_{id}^{k+1} = x_{\min\_\text{d}} + Z_{id}^{k+1}(x_{\max\_d} - x_{\min\_d}) \\ Z_{id}^{k+1} = \mu Z_{id}^{k}\left(1 - Z_{id}^{k}\right) \end{cases}. \tag{3}$$

In (3), $x_{\max\_d}/x_{\min\_d}$ is the upper and lower limits of the particle's position in the d dimension; μ represents an arbitrary number in the (0, 4) interval; and Z_{id}^{k} denotes the percentage of the position limit at the k iteration in the (0, 1) interval. We also introduced an adaptive algorithm to solve the premature defects and improve the model. The premature judgment is shown in Eq. (4) [16].

$$\sigma^{k} = \frac{1}{N}\sum_{i=1}^{N}\left(\frac{f_i^k - f_{\text{avg}}^k}{f}\right)^2. \tag{4}$$

In (4), f_i^k represents the variance of the particle swarm's fitness at k-th iteration; f_i^k is the fitness of the particle i at k-th iteration, and f_{avg}^k shows the mean value of particle i's fitness at the k-th iteration. Figure 2 is flow chart of the CQPSO algorithm.

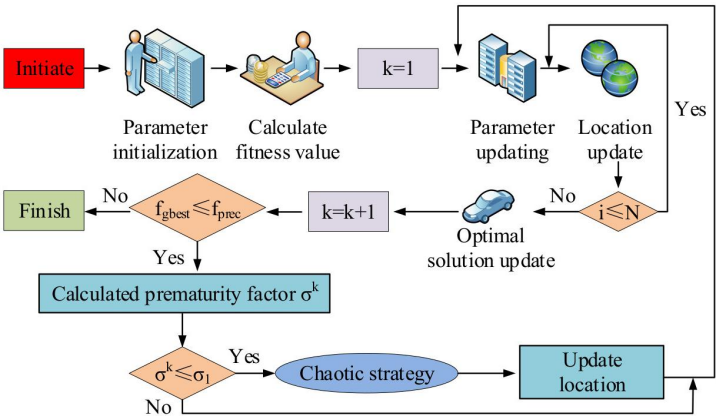

Fig. 2. Operation flow of CQPSO algorithm

The running process of CQPSO algorithm includes six steps. The first step is to initialize parameters and particle information, followed by particle updating and the fitness value calculation. Based on the termination condition, it will determine whether the global optimal value is less than the threshold. If the condition is not satisfied, then the process will proceed with the precocity factor judgment, thus forming a cycle. To strengthen the global search ability of the model, the moth-flame optimization (MFO) is introduced. This intelligent algorithm is based on the principle that moths do not fly directly toward light sources but spiral in to light sources. The moth population M and the flame population F are shown in matrix (5) [17].

$$\begin{cases} M = \begin{bmatrix} m_{1,1} & m_{1,2} & \cdots & m_{1,d} \\ m_{2,1} & m_{2,2} & \cdots & m_{2,d} \\ \cdots & \cdots & \cdots & \cdots \\ m_{N,1} & m_{N,2} & \cdots & m_{N,d} \end{bmatrix} \\ F = \begin{bmatrix} f_{1,1} & f_{1,2} & \cdots & f_{1,d} \\ f_{2,1} & f_{2,2} & \cdots & f_{2,d} \\ \cdots & \cdots & \cdots & \cdots \\ f_{N,1} & f_{N,2} & \cdots & f_{N,d} \end{bmatrix} \end{cases}. \tag{5}$$

The fitness matrices for the two populations are shown in matrix (6).

$$\begin{cases} OM = [OM_1, OM_2, \ldots, OM_N]^T \\ OF = [OF_1, OF_2, \ldots, OF_N]^T \end{cases}. \tag{6}$$

The population matrix has the same dimensions with the fitness matrix. The moths are equivalent to individuals who are looking for the best position and the flame is that position. Equation (7) shows how the moths update their positions.

$$\begin{cases} M_{id} = S\left(M_{id}, F_{jd}\right) \\ S(M_{id}, F_{jd}) = D_{ij\_d} \cdot {}^{bt_1} \cdot os(2\pi t_1) + F_{jd} \\ D_{ij\_d} = \left|M_{id} - F_{jd}\right| \end{cases}. \tag{7}$$

In (7), M_{id}/F_{jd} denotes the positions of moth and flame in the dimension of d; S represents the spiral function; D_{ij_d} is the absolute value of the distance between the moth and flame; b shows the definition of the logarithmic spiral shape; and t_1 is an arbitrary value in the interval [–1, 1]. It is used to judge the distance between the moth and the flame. When the value is –1, the moth and the flame are closest, and vice versa. To improve the performance of the model in global optimization seeking, it is necessary to order the flames by OF and approximate the flames in this way. By reducing the number of flames, the model will be better at local optimization seeking, as shown in Eq. (8).

$$f\_\text{no} = \text{round}\left(N - k\frac{N-1}{\text{Iter\_max}}\right). \tag{8}$$

In (8), f_no indicates the number of flames; Iter_max shows the maximum number of iterations; k is the current number of iterations; round represents the integer function, and N is the judgment value. When the number of flames is less than this value, the moths of the former f_no number are tracked, and the rest are constantly approaching. Figure 3 shows the flow chart of the MFO.

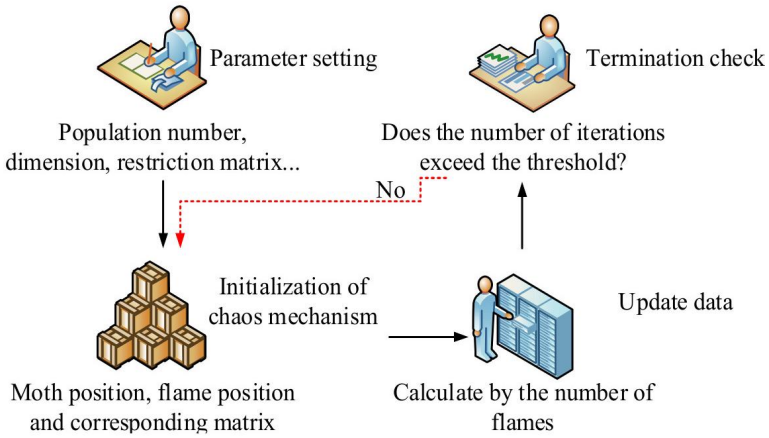

Fig. 3. Operation flow of MFO algorithm

There are four steps to operate the MFO algorithm. The first step is to initialize the number of moth populations and dimensions, and set the iteration threshold, the restriction matrix and other parameters. Then, a chaotic mechanism should be introduced to initialize and update the position of moths and flames, as well as the corresponding matrix. Next, the number of flames is calculated and the relevant position data is updated. When the number of iterations is greater than the threshold, the algorithm will stop running.

3.2. CQPSO-MFO and PV system MPP analysis and scenario-based optimization

To understand the relationship between the internal parameters and the single peak MPP, we need to convert the PV array output function to a display function of current and voltage using the Lambert W function, which is shown in Eq. (9) [18].

$$\begin{cases} I_{\text{array}} = \dfrac{R_p n_s N_{ss}(I_{ph} + I_o) - V_{\text{array}}}{n_s N_{ss}(R_s + R_p)} n_p N_{pp} - \dfrac{nV_T}{R_s} n_p N_{pp} \times W\left[Z_1\right] \\ V_{\text{array}} = R_p n_s N_{ss}(I_{ph} + I_o) - I_{\text{array}}(R_s + R_p)\left(\dfrac{n_s N_{ss}}{n_p N_{pp}}\right) - nV_T n_s N_{ss} \times W[Z_2] \end{cases}. \tag{9}$$

In Eq. (9), $I_{\text{array}}/V_{\text{array}}$ represents the current and voltage values of the PV array; R_p/R_s represents the resistance values of the PV module in series and parallel; n is the diode ideal factor; n_s/N_{ss} represents the number of cells in series of the module and the number of cells in series of the array; n_p/N_{pp} is the number of its corresponding parallel branch; I_{ph} is the photogenerated current of the battery; I_o stands for the diode reverse saturation current; V_T is the thermal voltage; W indicates the Lambert's W function, and Z_1/Z_2 denotes the calculation variables. The PV array power is shown in Eq. (10) [19].

$$\begin{aligned} P_{\text{array}} &= \frac{R_p n_s N_{ss}(I_{ph} + I_o)V_{\text{array}} - V_{\text{array}}^2}{n_s N_{ss}(R_s + R_p)} n_p N_{pp} - \frac{nV_T}{R_s} n_p N_{pp} V_{\text{array}} \times W[Z_1] = \\ &= R_p n_s N_{ss}(I_{ph} + I_o)I_{\text{array}} - I_{\text{array}}^2(R_s + R_p)\left(\frac{n_s N_{ss}}{n_p N_{pp}}\right) - nI_{\text{array}}V_T n_s N_{ss} \times W[Z_2]. \end{aligned} \tag{10}$$

Next, the current and voltage in Eq. (10) are derived so that the value is equal to 0. The final equations for the voltage and current at the MPP can be solved through iteration or algorithm. To address the scenario of strong uniform light, a maximum power tracking controller model is proposed. The model integrates the internal parameter method with the conductance incremental method (INC). INC is a traditional MPPT technique designed to regulate the control variables without duty cycle. The combination of the two techniques generates an offline parameter-based MPP tracking model with known internal parameters and Newtonian iterations. Thus, the tracking is achieved. The whole process is shown in Eq. (11).

$$R_{\text{load}} = \frac{R_{\text{input}}}{(1 - D)^2}. \tag{11}$$

In Eq. (11), R_{load} represents the load impedance; R_{input} stands for the input side resistance in the circuit; and D is the duty cycle. Equation (12) shows the input resistance at the maximum power point.

$$R_{\text{input@mpp}} = \frac{V_{@\text{mpp}}}{I_{@\text{mpp}}}. \tag{12}$$

In Eq. (12), $R_{\text{input@mpp}}$ denotes the input resistance of the MPP; and $/V_{@\text{mpp}}I_{@\text{mpp}}$ stands for the voltage and current of the MPP. Assuming that $R_{\text{load}} = R_{\text{input@mpp}}$, the duty cycle of the MPP can be obtained by Eq. (13).

$$D_{@mmp} = 1 - \sqrt{\frac{R_{\text{input@mpp}}}{R_{\text{load}}}}. \tag{13}$$

The input resistance at the MPP depends on values of the voltage and current at that point. Therefore, we proposed to adopt the offline parameter estimation approach, which can extract internal parameters under various operating conditions. The results will be stored in a parameter database (Fig. 4).

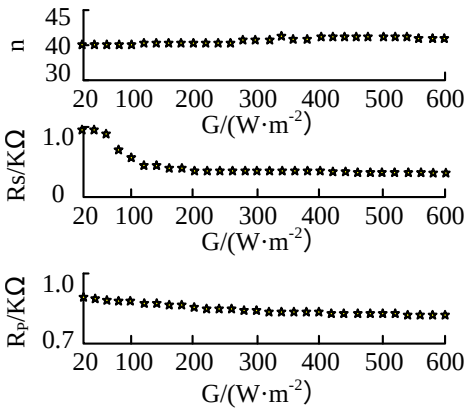

Fig. 4. Extraction of some internal parameters when the temperature is 25°

Figure 4 shows the results of the identification. The identified internal parameters are in line with the parameter trend. For example, PV module's parallel resistance is inversely proportional to the light intensity, so the trend is downward. In comparison, the photogenerated current of the cell is positively related to the light intensity and temperature [20]. The offline parameter approach should satisfy the restart detection condition before we calculate the short-circuit current parameter. By analyzing the photogenerated current parameters in the database, we will identify the nearest internal parameter. The characteristic curve of the PV cell array under standard test conditions (STCs) is shown in Fig. 5.

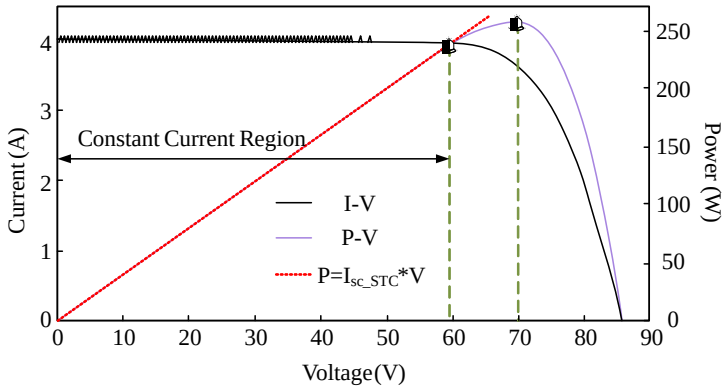

Fig. 5. Characteristic curve of photovoltaic cell array under standard test conditions (STCs)

According to Fig. 5, the current output of the PV array has an area of constant characteristics, where the fluctuation is small and almost negligible. The model regards it as a short-circuit current. When we need to measure the short-circuit current, the operating point can be moved to this area. To improve the stability of the model's operation under different temperatures, the module temperature is used as the basis for parameter measurement [21]. However, the model still has a steady-state oscillation. To help the model maintain a steady-state condition, in which variables do not change, until restart, we have introduced the concept of direction flag. Then, the absolute value of the direction sum of the control variables during the three cycles is calculated. The results will serve as the basis to determine whether the working point reaches the steady state, as shown in Eq. (14).

$$\begin{cases} \left|\sum_{i=1}^{3} \text{slope}\,(i)\right| = 1 \\ \sum_{i=2}^{3} \text{slope}\,(i) = 0 \end{cases} . \tag{14}$$

The slope value is +1 when the control variable increases. It becomes –1 when the control variable goes down. If the operating point meets the conditions of the equation above, it is shown as a steady-state oscillation phase. To make the model more accurate, the perturbation step size needs to be reduced and vice versa. Although the offline parameter approach can address single-peak scenarios, it cannot provide parameter feedback of PV arrays in real time. Thus, the perturbation-and-observation (PO) method is adopted for further optimization. Figure 6 shows the MATLAB model.

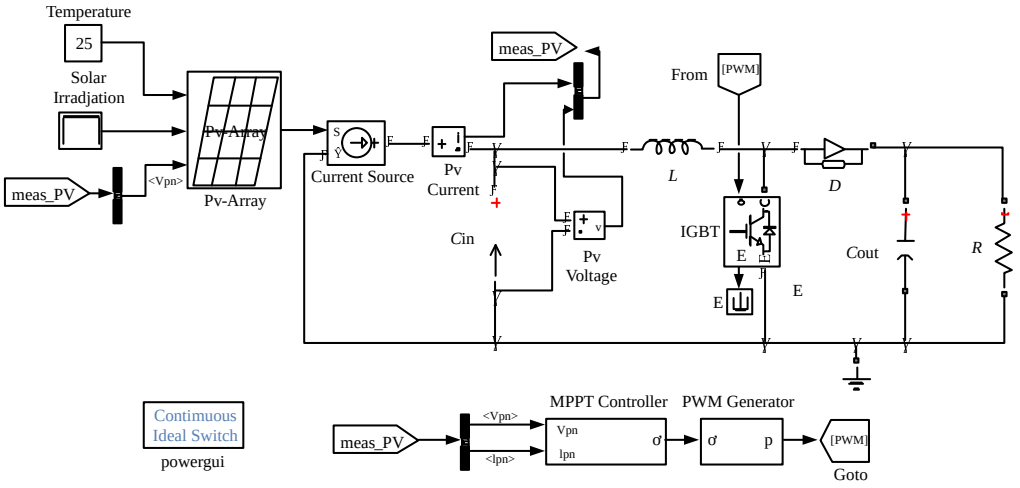

Fig. 6. MATLAB model diagram

For example, each module of the 10 PV module arrays has different light intensity. The characteristic output curve has 10 peaks. The internal parameters such as short-circuit current and open-circuit voltage of the arrays can be obtained by dividing the demarcation points. The voltage of each service data point (SDP) is as shown in Eq. (15) [22].

$$V_{@\text{SDP}_i} = (i-1)V_{oc\_\text{mod}} + V_{\text{mpp\_mod}} - (N_{ss} - i)V_d. \tag{15}$$

In Eq. (15), $V_{@\mathrm{SDP}_i}$ denotes the voltage value of any SDP point; i stands for any area; V_{mpp_mod} is the MPP voltage; V_{oc_mod} represents the open circuit voltage; and V_d is the control voltage. To obtain the coefficients of the short-circuit current ratio $\alpha_{@i,j}$ at different SDP points, we need to first calculate the short-circuit current parameters. Then, we need to use local shading to determine the regional step. The minimum regional variable is also introduced to improve the efficiency. Figure 7 shows the MPPT process.

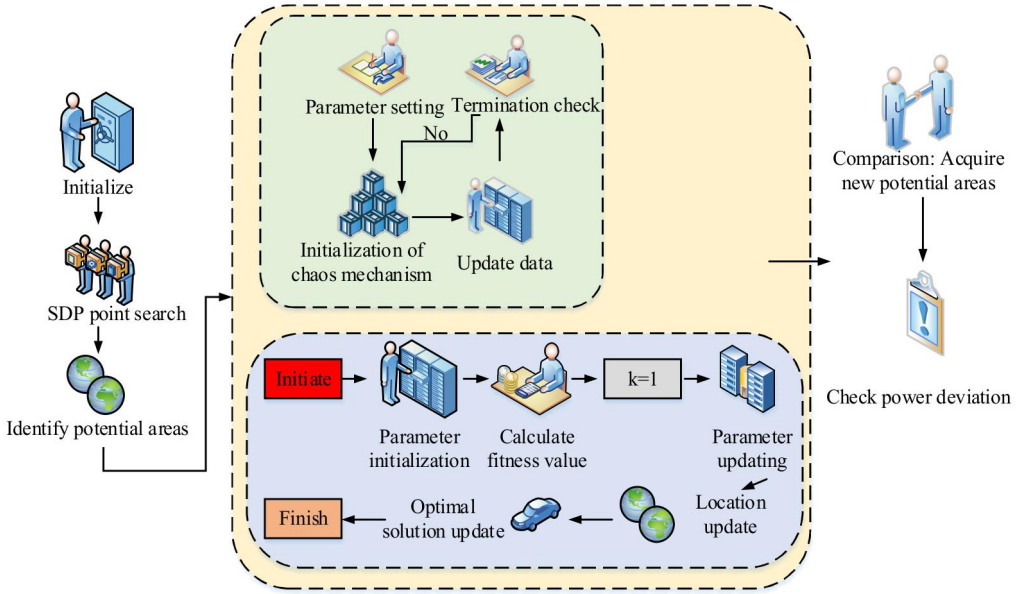

Fig. 7. MPPT process based on CQPSO-MFO real-time internal parameter extraction

The P&O method and the CQPSO-MFO algorithm require multiple sets of regional current and voltage values to extract and identify internal parameters. Finally, the regional and potential peak voltages are calculated and their corresponding short-circuit voltage ratio coefficients are computed to form the new potential range.

4. Performance analysis of CQPSO-MFO hybrid algorithm in MPPT real-time tracking application

The goal of this section is to verify the performance of the proposed tracking controller, which combines both the CQPSO-MFO algorithm and the traditional MPPT method. The performance of the CQPSO-MFO algorithm is analyzed through an experiment. In the experiment, the process of the offline parameter extraction and the real-time parameter extraction are simulated respectively.

4.1. Simulation analysis of the performance of hybrid optimization algorithm based on CQPSO-MFO

To verify the performance of the internal parameter extraction algorithm, the study introduces several algorithms as the control group. The algorithms include the differential evolution algorithm (DE), the soft actor-critic particle swarm optimization (SACPSO) algorithm based on flexible action-evaluation, and the simulated annealing (SA) algorithm. Table 1 shows the experimental environment and parameter settings.

Table 1. Experimental environment and parameter Settings

Name		Settings
Population size		100
Iteration maximum		500
Target fitness value		0.05
Upper limit of individual position		[1.256, 1e–4, 16, 0.5, 1000]
Lower limit of individual position		[1.246, 1e–10, 10, 0, 0]
Buck-boost converter	Input capacitance	470 μF
	Output capacitance	220 μF
	Inductance	1 mH
	Switching frequency	10 kHz
Simulation platform		MATLAB/Simulink
MPPT controller sampling time		0.5 s

After 50 iterations of each algorithm, we have obtained the final parameter identification results. Figure 8 shows the results of each algorithm model.

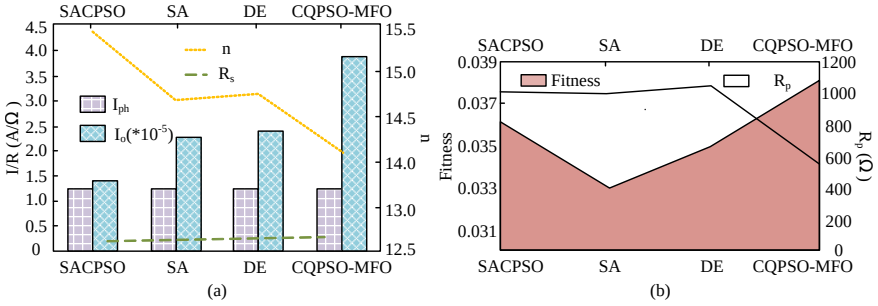

Fig. 8. Parameter identification results of each algorithm model: internal parameters such as current of each algorithm (a); internal parameters and fitness of each algorithm (b)

Figure 8(a) shows the PV module shunt resistance R_p, the series resistance R_s, the diode ideal factor n, the photogenerated current I_{ph}, and the diode reverse saturation current I_o of the PV array. The fitness values of all the models are also shown. The algorithms have been used to identify the photogenerated current and series resistance. According to the results, the mean values are 1.25 and

0.23 for each, which do not differ much. The proposed CQPSO-MFO algorithm performs much better in identifying the shunt resistance, the diode ideal factor, and the diode reverse saturation current. The identified values are 548.292 Ω, 14.923, and $3.876 \cdot 10^{-5}$, respectively. Their parallel resistance values are reduced by 80.16% on average. and all the three parameters are inversely proportional to the light intensity. Therefore, the CQPSO-MFO algorithm is the most competent algorithm in identifying the internal parameters. According to Fig. 8(b), the fitness values of the algorithms are 0.036, 0.033, 0.035, and 0.038, respectively. The proposed CQPSO-MFO algorithm can obtain the optimal fitness, which is 8.77% higher than other algorithms. Based on the internal parameters obtained by each algorithm, we can fit the current-voltage curves and the power-voltage curves, as shown in Fig. 9.

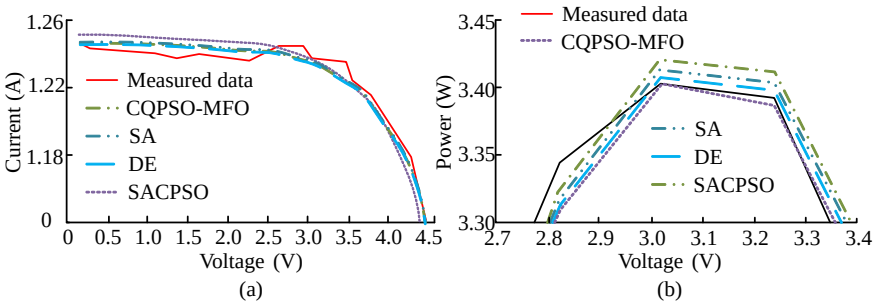

Fig. 9. Comparison of fitting curves of each algorithm model: current-voltage fitting curve (a); power-voltage fitting curve (b)

According to Fig. 9(a), when the voltage value is at the [0, 3] interval, the fitting curve approximates the constant current and the measured data shows a more noticeable oscillation. Although each model's fitting results vary slightly, they are all closer to the measured data and smoother. The fitting results of the SACPSO algorithm deviate more from the measured value. For example, at the voltage of 1.5 V, its deviation is 0.81% more than other algorithms. In the subsequent regions, the fitting curves of the algorithms gradually converge. According to Fig. 9(b), all algorithms' fitted power-voltage curves are accurate. The difference between the measured MPP and the actual value is small. When we take a close look, the proposed CQPSO-MFO algorithm has less error than others. Its identification error is only 0.001%, which is 5% lower than other algorithms on average. In summary, although all the algorithms can accurately fit the internal parameters, the CQPSO-MFO algorithm performs the best.

4.2. Simulation analysis of CQPSO-MFO optimization model applied in MPPT of PV systems

Experiments were carried out to validate the MPPT model, which were based on offline parameters. The experiments used traditional incremental conductance (TINC) method and constant current tracking (CCT) method, and both of which were not optimized. The temperature of the battery was set to be 50 degrees and its resistive load parameter was set to be 120 Ω. Figure 10 shows the results.

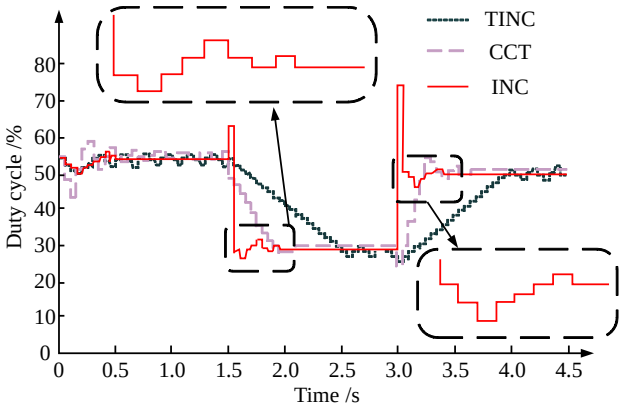

Fig. 10. Performance comparison of MPPT model based on offline parameters

Figure 10 shows the duty cycle curves of each model. Case 1 shows that, at a simulation time of 1.5 s, the light intensity drops from 1000 W/m^2 to 430 W/m^2. The tracking time of TINC, CCT, and the optimized INC method adopted in this study is 0.6 s, 0.2 s, and 0.1 s, respectively. The model proposed by the study has the shortest processing time, which 33.3% shorter than the average time used by the other two methods. When there is a sudden change in light intensity, the absolute value of the proposed model's power deviation is greater than the threshold value. The duty cycle rises from 62.1% to 68.83% and the voltage stays at 33.67 V. The operating point is a constant current, so 1.73 A will be regarded as a short-circuit current. Based on the database, the parameter can be calculated when the light intensity is 420 W/m^2 and the error is 2.3%. Case 2 also has a sudden change in light intensity, with the simulation time 3.0 s. Following the same calculation process, we can obtain each model's performance, as shown in Fig. 11.

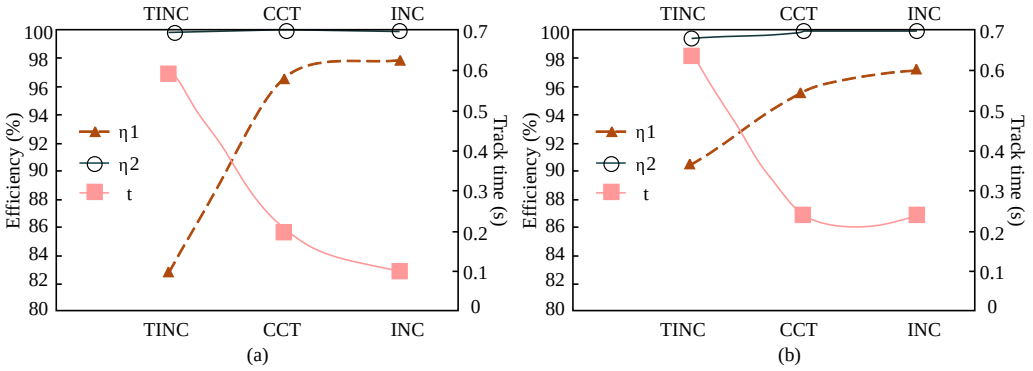

Fig. 11. Trace performance of each model in different cases: case 1 (a); case 2 (b)

According to Fig. 11(a), in Case 1, all three methods have excellent steady-state accuracy ($\eta 2$), reaching over 99%. However, the values of their tracking efficiency ($\eta 1$) are significantly different. TINC, CCT, and the optimized INC method's efficiency values are 82.8%, 96.5%, and 97.7%, respectively. The average tracking efficiency of the optimized INC method is 8.05% higher

than other methods. In Case 2, of which the results are shown in Fig. 11(b), the tracking time of TINC and CCT, and the optimized INC method is 0.55 s and 0.2 s, respectively. The three methods' steady-state accuracy ($\eta 2$) are above 99%, and their average tracking efficiencies $\eta 1$ are 89.8%, 95.2%, and 96.9%, respectively. Figures 10 and 11 compare the tracking time and tracking efficiency of different INC methods. According to the results, the proposed INC method requires the shortest processing time and can adapt better to the sudden change of light intensity. Its power deviation is small. Although all the methods perform well in terms of the steady-state accuracy, the optimized INC method has the highest average tracking efficiency. Therefore, the proposed off-line parameter MPPT method based on INC meets the requirements of both time and accuracy. To analyze the real-time parametric MPPT method, the study has conducted experiments to compare the performances of the enhanced adaptive perturbation-and-observation (EAPO) algorithm, the differential evolution algorithm (DE), the effective hybrid perturbation-and-observation (EHPO) algorithm, and the overall distribution particle swarm optimization (ODPSO) algorithm. The results are shown in Table 2.

Table 2. Application effects of each model in real-time parameter MPPT

Index	**EAPO**	**DE**	**EHPO**	**ODPSO**	**PO-CQPSO-MFO**	**PSO**
t	1.31	1.56	2.31	1.71	2.39	8.84
$\eta 1$	92.81	87.23	82.56	89.31	86.58	69.92
$\eta 2$	99.79	93.80	99.78	96.58	99.84	76.43
Tracking result	Success	Loss	Success	Loss	Success	Loss

According to Table 2, both DE algorithm and ODPSO algorithm are unable to track the maximum power point (MPP), because both of them fall into the local optimum. When the power of each region is less than 5%, the DE algorithm will terminate. This makes the model less accurate at steady state. This is the lowest among all the algorithms. EAPO has a shorter processing time and a higher tracking efficiency due to its simple structure. However, it is unable to deal with temperature variations and may generate inaccurate results during the measurement. After we compared the performances of the traditional PSO algorithm and optimized PSO algorithm, we discovered that the optimized PSO algorithm's running time was reduced by 72.96%. Besides, its average tracking efficiency was improved by 16.66% and its steady-state accuracy was enhanced by 23.41%. Therefore, the optimization effect of the traditional PSO algorithm is very significant, with shorter running time and higher accuracy. In summary, the PO-CQPSO-MFO tracking model proposed in the study has the best performance, with the highest tracking speed and steady-state accuracy.

5. Conclusion

To enhance the power generation efficiency of the PV array system, a maximum power point tracking controller model based on chaotic quantum particle swarm-mothballing hybrid algorithm has been proposed in this study. The model is optimized and combined with offline and real-time parameters. To test its validity, we have conducted various experiments on the

MATLAB/Simulink platform. The first step is to verify the performance of the internal parameter identification algorithm. The results show that the CQPSO-MFO algorithm proposed in the study is best at identifying parameters. Its average shunt resistance is 80.16% lower and its adaptation value is 8.77% higher than other algorithms. In terms of fitting curves to their corresponding outputs, all algorithms perform well in current-voltage fitting. As for the power-voltage fitting, the CQPSO-MFO algorithm has an 0.001% identification error at the MPP point. This is 5% lower than other algorithms on average. According to our simulation of MPPT controller based on internal parameter extraction, the steady-state accuracy against the offline parameter tracking controllers reached more than 99%. The optimized INC method had 8.05% higher average tracking efficiency than other methods on average. Moreover, its running time was 33.3% shorter than other methods on average. As for the tracking of real-time parameters, the PO-CQPSO-MFO model is not optimal, but it has the best overall performance, with a higher tracking speed and accuracy at the maximum power point. The model's tracking time, steady-state accuracy, and average tracking efficiency are 2.39 s, 99.84%, and 86.58%, respectively. This study only covers MPPT controller's application in off-grid DC PV systems. Future studies should focus on its application in grid connected PV Systems. Moreover, integrating battery energy storage systems can increase the amount of energy stored and improve the system's adaptability to load fluctuations. At the same time, improving the conversion efficiency of independent power generation systems (such as using more efficient solar panels or wind turbines) is also necessary, because it can reduce the amount of resources and equipment required. What's more, we need to ensure that inverters and other grid-connected interface equipment comply with the latest technical safety standards and have good power quality control. Following this strategy, this technique can be further applied to the grid-connected system.

References

[1] Herrando M., Elduque D., Javierre C., Fueyo N., *Life Cycle Assessment of solar energy systems for the provision of heating, cooling and electricity in buildings: A comparative analysis*, Energy Conversion and Management, vol. 257, no. 1, 115402 (2022), DOI: 10.1016/j.enconman.2022.115402.

[2] Raina G., Sinha S., Saini G., Sharma S., Malik P., Thakur N.S., *Assessment of photovoltaic power generation using fin augmented passive cooling technique for different climates*, Sustainable Energy Technologies and Assessments, vol. 52, no. 8, pp. 102095–102102 (2022), DOI: 10.1016/j.seta.2022.102095.

[3] Sun T., Shan M., Rong X., Yang X., *Estimating the spatial distribution of solar photovoltaic power generation potential on different types of rural rooftops using a deep learning network applied to satellite images*, Applied Energy, vol. 315, no. 3, pp. 119025–19035 (2022), DOI: 10.1016/j.apenergy.2022.119025.

[4] Asoh D.A., Noumsi B.D., Mbinkar E.N., *Maximum power point tracking using the incremental conductance algorithm for PV systems operating in rapidly changing environmental conditions*, Smart Grid and Renewable Energy, vol. 13, no. 5, pp. 89–108 (2022), DOI: 10.4236/sgre.2022.135006.

[5] Rerhrhaye F., Lahlouh I., Ennaciri Y., Benzazah C., Akkary A.E., Sefiani N., *New solar MPPT control technique based on incremental conductance and multi-objective ant colony optimization*, International Review of Automatic Control, vol. 15, no. 3, pp. 113–121 (2022), DOI: 10.15866/ireaco.v15i3.22076.

[6] Mishra J., Das S., Kumar D., Pattnaik M., *A novel auto-tuned adaptive frequency and adaptive step-size incremental conductance MPPT algorithm for photovoltaic system*, International Transactions on Electrical Energy Systems, vol. 31, no. 10, 12813 (2021), DOI: 10.1002/2050-7038.12813.

[7] Dehghani M., Taghipour M., Gharehpetian G.B., Abedi M., *Optimized fuzzy controller for MPPT of grid-connected PV systems in rapidly changing atmospheric conditions*, Journal of Modern Power Systems and Clean Energy, vol. 9, no. 2, pp. 376–383 (2021), DOI: 10.35833/MPCE.2019.000086.

[8] Lei X., *Novel sub-area maximum power point tracking method based on improved variable-step-size perturbation and observation*, Sensors and Materials: An International Journal on Sensor Technology, vol. 34, no. 4, pp. 1433–1444 (2022), DOI: 10.18494/SAM3655.

[9] Zhang L., Wang Z., Cao P., *A maximum power point tracking algorithm of load current maximization-perturbation and observation method with variable step size*, Symmetry, vol. 12, no. 2, pp. 244–254 (2020), DOI: 10.3390/sym12020244.

[10] Gharpure S., Ghodinde K.A., Deshpande A., Patil S.L., *MPPT for thermoelectric generator using modified perturbation and observation method*, International Conference on Advances in Electrical and Computer Technologies, vol. 711, no. 1, pp. 1293–1304 (2020), DOI: 10.1007/978-981-15-9019-1_105.

[11] Yan Y., Wang B., Wang C., Zhao D., Xiao C., *Adaptive maximum power point tracking based on Kalman filter for hydrogen fuel cell in hybrid unmanned aerial vehicle applications*, International Journal of Hydrogen Energy, vol. 48, no. 66, pp. 25939–25957 (2023), DOI: 10.1016/j.ijhydene.2023.03.288.

[12] Wang L., Wang H., Fu M., Liang J., Liu Y., *A three-port energy router for grid-tied pv generation systems with optimized control methods*, IEEE Transactions on Power Electronics, vol. 38, no. 1, pp. 1218–1231 (2023), DOI: 10.1109/TPEL.2022.3202873.

[13] Pendem S.R., Mikkili S., *Assessment of cross-coupling effects in PV String-integrated-converters with P&O MPPT algorithm under various partial shading patterns*, Journal of Electric Power and Energy Systems of the Chinese Society of Electrical Engineering, vol. 8, no. 4, pp. 63–70 (2022), DOI: 10.17775/CSEEJPES.2019.03330.

[14] Dian S., Zhong J., Guo B., Liu J., Guo R., *A smooth path planning method for mobile robot using a BES-incorporated modified QPSO algorithm*, Expert Systems with Application, vol. 208, no. 9, pp. 118256–118271 (2022), DOI: 10.1016/j.eswa.2022.118256.

[15] Wan L., Li H., Chen Y., Li C., *Rolling bearing fault prediction method based on QPSO-BP neural network and dempster-shafer evidence theory*, Energies, vol. 13, no. 5, pp. 1094–1117 (2020), DOI: 10.3390/en13051094.

[16] Usman A.M., Abdullah M.K., *An assessment of building energy consumption characteristics using analytical energy and carbon footprint assessment model*, Green and Low-Carbon Economy, vol. 1, no. 1, pp. 28–40 (2023), DOI: 10.47852/bonviewGLCE3202545.

[17] Kashyap A.K., Parhi D.R., Kumar P.B., *Route outlining of humanoid robot on flat surface using MFO aided artificial potential field approach*, Proceedings of the Institution of Mechanical Engineers, Part B: Journal of Engineering Manufacture, vol. 236, no. 6, pp. 758–769 (2022), DOI: 10.1177/09544054211041.

[18] Fang Y., Luo B., Zhao T., Dong H., Jiang B., Liu Q., *ST-SIGMA: Spatio-temporal semantics and interaction graph aggregation for multi-agent perception and trajectory forecasting*, CAAI Transactions on Intelligence Technology, vol. 7, no. 4, pp. 744–757 (2022), DOI: 10.1049/cit2.12145.

[19] Pravalika J., Pakkiraiah B., Rekha M., *Improved performance of an asynchronous motor drive with a new modified incremental conductance based MPPT Controller*, 3rd International Conference on Design and Manufacturing Aspects for Sustainable Energy, Hyderabad, India, vol. 309, no. 01183 (2021), DOI: 10.1051/e3sconf/202130901183.

[20] Antony R.S., Giftson S.G., *BOSS-D-RBFN: Boosted Salp Swarm optimization based Deep RBFN for MPPT under partial shading condition in photovoltaic systems*, Optik, vol. 1, no. 259, pp. 168876–168896 (2022), DOI: 10.1016/j.ijleo.2022.168876.

[21] Rajesh K., *Radial basis function neural network MPPT controller-based microgrid for hybrid stand-alone energy system used for irrigation*, Circuit World, vol. 49, no. 2, pp. 251–266 (2023), DOI: 10.1108/CW-03-2022-0076.

[22] Ghoshal S., Banerjee S., Chanda C.K., *Modelling and performance evaluation of MPPT-based PMSG wind energy conversion system with different interfaces in MATLAB/Simulink environment*, International Journal of Performability Engineering, vol. 18, no. 1, pp. 63–70 (2022), DOI: 10.23940/ijpe.22.01.p8.6370.